MARSIS: Mars Advanced Radar for Subsurface and Ionosphere Sounding

G. Picardi[1], D. Biccari[1], R. Seu[1], J. Plaut[2], W.T.K. Johnson[2], R.L. Jordan[2], A. Safaeinili[2], D.A. Gurnett[3], R. Huff[3], R. Orosei[4], O. Bombaci[5], D. Calabrese[5] & E. Zampolini[5]

[1]*Infocom Department, 'La Sapienza' University of Rome, Via Eudossiana 18, I-00184 Rome, Italy*
Email: aclr@aerov.jussieu.fr
[2]*Jet Propulsion Laboratory, 4800 Oak Grove Drive, Pasadena, CA 91109, USA*
[3]*Department of Physics and Astronomy, University of Iowa, Iowa City, IW 52242-1447, USA*
[4]*CNR/IAS, Planetology Department, Via del Fosso di Cavaliere, I-00133 Rome, Italy*
[5]*Alenia Spazio S.p.A., Via Saccomuro 24, I-00131 Rome, Italy*

This paper describes the science background, design principles and the expected performance of the Mars Advanced Radar for Subsurface and Ionosphere Sounding (MARSIS), developed by a team of Italian and US researchers and industrial partners to fly on the ESA Mars Express orbiter. The unique capability of sounding the martian environment with coherent trains of long-wavelength wide-band pulses, together with extensive onboard processing, will allow the collection of a large amount of significant data about the subsurface, surface and ionosphere. Analysis of these data will allow the detection and 3-D mapping of subsurface structures down to several kilometres below the surface, the estimation of large-scale topography, roughness and reflectivity of the surface at wavelengths never used before, and the production of global and high-resolution profiles of the ionospheric electron density (day and night). Finally, the MARSIS frequency-agile design allow the sounding parameters to be tuned in response to changes in solar illumination conditions, the latitude and other factors, allowing global coverage to be achieved within the Mars Express baseline orbit and mission duration.

1. Introduction

The set of scientific objectives for MARSIS was defined in the context of the objectives of the Mars Express mission and within the more general frame of the open issues in Mars studies. The primary objective is to map the distribution of liquid and solid water in the upper portions of the crust of Mars (Carr, 1996). Detection of such water reservoirs will address key issues in the hydrologic, geologic, climatic and possible biologic evolution of Mars, including the current and past global inventory of water, mechanisms of transport and storage of water, the role of liquid water and ice in shaping the landscape of Mars, the stability of liquid water and ice at the surface as an indication of climatic conditions, and the implications of the hydrologic history for the evolution of possible martian ecosystems.

Three secondary objectives are also defined for MARSIS: subsurface geologic probing, surface characterisation and ionosphere sounding. The first is to probe the subsurface of Mars, to characterise and map geologic units and structures in the third dimension. The second is to acquire information about the surface: to characterise the surface roughness at scales of tens of metres to kilometres, to measure the radar reflection coefficient of the upper surface layer, and to generate a topographic map of the surface at approximately 10 km lateral resolution. The final secondary objective is to use MARSIS as an ionosphere sounder to characterise the interactions of the

solar wind with the ionosphere and upper atmosphere of Mars. Radar studies of the ionosphere will allow global measurements of the ionosphere electron density and investigation of the influence of the Sun and the solar wind on the ionosphere.

2. Composition Models of the Upper Layers

In this section, models of the composition of the upper layers of Mars are described, based on the recent literature and classical Mars studies.

The state and the distribution of H_2O in the martian megaregolith are a function of crustal thermal conductivity, geothermal heat flow, ground-ice melting temperature and the mean temperature at the surface (this last is the only quantity varying systematically with latitude). These factors determine the thickness of the cryosphere, which is the layer where the temperature remains continuously below the freezing point of H_2O. Although the mean annual surface temperatures vary from about 220K at the equator to about 155K at the poles, the annual and secular surface temperature variations determine periodic freezing and melting of any H_2O present down to a depth of about 100 m. The cryosphere extends below this 'active layer' to the depth where the heat flux from the interior of the planet raises the temperature above the melting point of ground-water ice. Below the cryosphere, H_2O in the pore space can only be in liquid form.

Estimates of the depth of the melting isotherm range from 0 km to 11.0 km at the equator, and from 1.2 km to 24 km at the poles, according to different values of the parameters found in the literature. Liquid water may persist only below such depths; moreover, liquid water would diffuse towards the bottom of the regolith layer and thus could lay further below, although local conditions may still offset the above considerations. A nominal depth in the range 0-5000 m is assumed.

Estimates of the desiccation of the martian megaregolith, via ice sublimation in the cryosphere, yield values of the depth at which ice is still present ranging from zero to several hundred metres. A nominal depth in the range 0-1000 m is assumed.

The interfaces most likely to be detected by MARSIS, being closer to the surface, are the contact between the desiccated regolith and the permafrost, and the interface between a subterranean reservoir of liquid water and the cryosphere. These are the basic scenarios for the detection and identification of water-related interfaces in the martian subsurface.

The structure of the martian crust is the result of many different processes, given the complex geological history of the planet. However, it appears that the most significant on a global scale are impact processes, which have played a major role in the structural evolution of the crust by producing and dispersing large quantities of ejecta, and by fracturing the surrounding and underlying basement. It is estimated that, over the course of martian geologic history, the volume of ejecta produced by impacts was sufficient to have created a global blanket of debris up to 2 km thick. It is likely that this ejecta layer is discontinuously interbedded with volcanic flows, weathering products and sedimentary deposits, all overlying a heavily fractured basement.

A 50% surface porosity of the regolith is consistent with estimates of the bulk porosity of martian soil as analysed by the Viking Landers. A value this high requires that the regolith has undergone a significant degree of weathering. A lower bound for the surface porosity can be taken at 20%, derived from the measured porosity of lunar breccias. An equation of the decline of porosity with depth owing to the lithostatic pressure can be obtained by adapting a similar equation devised for the Moon, based on seismic data unavailable for Mars. The equation is of the form:

$$\Phi(z) = \Phi(0)\, e^{-\frac{z}{K}} \qquad (1)$$

where $\Phi(z)$ is the porosity at depth z, and K is a decay constant that, for Mars, can be computed by scaling the measured lunar decay constant for the ratio between the lunar and martian surface gravitational acceleration, under the assumption of comparable crust densities. The resulting value for Mars is $K = 2.8$ km.

Table 1. Dielectric properties of the subsurface material.

	Crust Material		*Pore-Filling Material*	
	Andesite	*Basalt*	*Water Ice*	*Liquid Water*
ε_r	3.5	7.1	3.15	88
tan δ	0.005	0.014	0.00022	0.0001

Table 2. Value ranges of the surface geometric parameters.

Large-Scale Model		*Small-Scale Model*	
rms slope	*correlation length*	*rms slope*	*rms height*
0.01-0.1 rad (0.57-5.7°)	200-3000 m	0.1-0.6 rad (5.7-34.3°)	0.1-1 m

It appears almost certain from morphologic and chemical evidence, as well as from SNC meteorites, that the martian surface is primarily basaltic. However, it could have a thin veneer of younger volcanics overlying a primitive crust. Whether this primitive crust is basaltic, anorthositic like the Moon, granodioritic like the Earth's continents or some other kind of composition, is unknown. The NASA Pathfinder APXS analyses of rocks and soils confirm the basaltic nature of Mars' surface. Chemical classifications of lavas show that the Barnacle Bill and Yogi rocks are distinct from basaltic martian meteorites. These rocks plot in or near the field of andesites, a type of lava common at continental margins on Earth. Although a multitude of different chemical compositions is present at the surface of Mars, it is necessary to select a few representative materials as most meaningful for electromagnetic studies. Given the above considerations about the nature of the martian crust, andesite and basalt were chosen because their dielectric constants are end-members of the range within which the martian surface materials may vary.

The dielectric properties of the crust end-member materials, together with those of the water and ice filling the pores, are listed in Table 1.

To summarise, the reference models representing the two most likely detection scenarios for a Mars orbital sounder at km depths are (Fig. 1):

Ice/water interface detection. According to the model, the porosity of the martian megaregolith is maximum at the surface and its decay with increasing depth is given by the exponential law in Eq. (1). The pores are filled with ice from the surface down to a depth below which liquid water is stable and becomes the pore-filling material. The change causes a discontinuity of the overall dielectric constant, which can be detected by the radar sounder. The ice/water interface is believed to be at a depth of between 0 m and 5000 m.

Dry/ice interface detection. This model is based on the same assumptions as the ice/water model with respect to the megaregolith properties. However, the pore-filling material here is considered to be gas or some other vacuum-equivalent material up to a certain depth below which ice fills the pores. Hence the interface to be detected is between dry regolith and ice-filled regolith, expected to be at a depth of between 0 m and 1000 m.

These models will be used to estimate the penetration performance under typical MARSIS operating conditions.

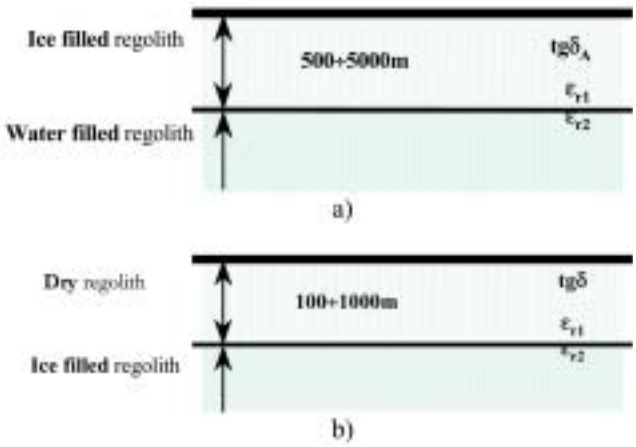

Fig. 1. Martian crust stratification models. Simple 2-layer structures are proposed. The discontinuity is created by a change in the pore-filling material. a: ice/water interface detection; b: dry/ice interface detection.

3. Surface Characterisation

Images of the surface from the Viking Landers and Mars Pathfinder depict a gently undulating surface strewn with rocks ranging in size from a few centimetres to metres. Although these images cover only a minute portion of the planet, Mars' thermal and radar properties have prompted extensive modelling of a rock population scattered over the entire surface. The surface geometric structure is thus characterised in terms of a *large-scale* morphology on which a *small-scale* geometric structure, of rocks, is superimposed. It is assumed that the surface can be described as a random distribution of heights, characterised by a variance σ_h, a correlation length L and a local surface rms slope m_s. By assuming that the height distribution is Gaussian, then $m_s = \sqrt{2}\,\sigma_h / L$, so that the distribution is completely determined once the values of two of these parameters are known. The terms large-scale and small-scale refer to different approximations in the modelling of the radar backscattering coefficient; the divide between large-scale and small-scale is essentially the radar wavelength.

Topographic data can be used to derive the large-scale geometry of the surface. The global topographic maps of Mars currently available were compiled from several types of measurements with different resolutions and sources of uncertainties. These data do not provide a complete, global picture of Mars' topography, but allow the inference that elevation changes, although relevant in magnitude, do not involve average slopes greater than 5° (0.1 rad), and often much less. Also, the correlation lengths for the topography appear to be rather large, perhaps of the order of tens of kilometres.

To characterise the surface geometry at scales smaller than the radar resolutions, it is necessary to use proper data sets: measured values for Mars are in the range 0.7-13°, averaging 2°, with a remarkable diversity from place to place over the surface. Such values refer to scales that, according to model interpretations, range from a few tens to a few hundred metres.

To summarise, plausible ranges for the parameters describing the surface geometry are listed in Table 2.

Recent attempts to describe the structure of planetary surfaces by means of fractals have also been taken into account. Tests on MGS/MOLA data have shown that the Hurst exponent (H) with very high probability lies in the range 0.7-1 and the rms slope ($s(\Delta x)$) extrapolated with a lag $\Delta x = 166$ m is lower than 0.05.

4. Characterisation of the Ionosphere

The study of the martian ionosphere is important not only as a topic in its own right, but also because the ionosphere has a strong influence on the subsurface and surface soundings. Electromagnetic radiation cannot propagate through an ionised gas at frequencies below the electron plasma frequency, given by $f_p = 8980\,\sqrt{N_e}$ Hz, where

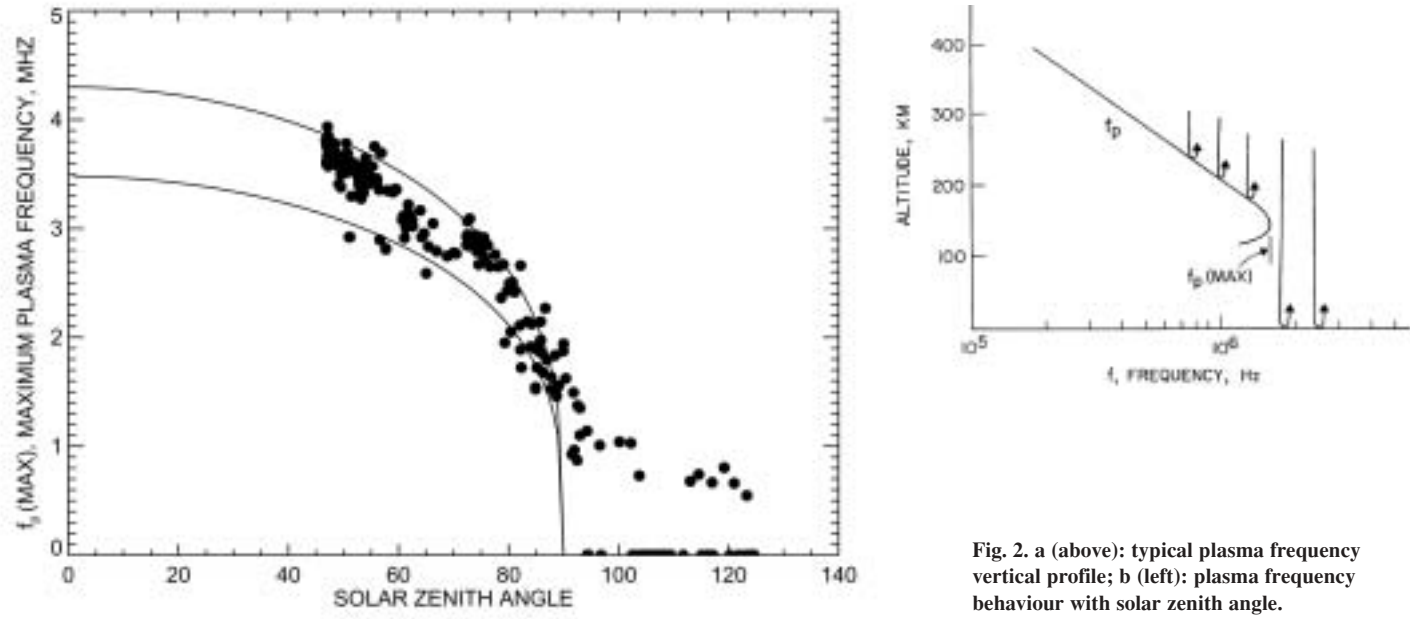

Fig. 2. a (above): typical plasma frequency vertical profile; b (left): plasma frequency behaviour with solar zenith angle.

N_e is the electron number density in cm^{-3}. A typical profile of the electron plasma frequency in the dayside martian ionosphere is shown in Fig. 2a, based on plasma density measurements from the Viking Landers (Hanson, 1977). Usually the electron plasma frequency on the dayside of Mars has a single, well-defined maximum, at an altitude of 125-150 km. Radio waves incident vertically on the ionosphere are reflected at the point where the wave frequency is equal to the electron plasma frequency. Transmission through the ionosphere is possible only at frequencies above the maximum electron plasma frequency in the ionosphere, f_p (max). Figure 2b shows a plot of f_p (max) versus solar zenith angle. The solid dots give the plasma frequency obtained from radio occultation measurements (Zhang et al., 1990a; 1990b), and the solid lines give extrapolations using the Chapman theory of planetary ionospheres.

Subsurface soundings are possible only at frequencies greater than f_p (max). Since they require frequencies as low as possible, the global distribution of the ionospheric electron density (hence plasma frequency) becomes an important factor in selecting the operating frequency of the sounder and the optimal orbital strategy for data collection. The lowest frequency that can penetrate the martian ionosphere varies from about 4 MHz on the dayside to somewhat below 1 MHz on the nightside. Clearly, the best region for carrying out subsurface soundings is on the nightside, at solar zenith angles greater than 90°. Unfortunately, very little is known about the ionosphere on the nightside. A typical nightside maximum plasma frequency appears to be about 800 kHz. From our knowledge of the ionosphere of Venus, for which better nightside electron density measurements are available, it is likely that there are isolated regions on the nightside of Mars where the plasma frequency extends well below 800 kHz.

Even when the sounding frequency is above f_p (max), the ionosphere still has an effect on the radar signal. As is well known (Stix, 1964), the index of refraction for an electromagnetic wave propagating through an unmagnetised plasma is given by $n = [1-(f_p/f)^2]^{1/2}$. Even at frequencies several times the plasma frequency, the index of refraction has a noticeable deviation from the free-space value of $n = 1$. This deviation causes a frequency-dependent time delay, called dispersion, that distorts the shape of the radar pulse. It is easily demonstrated that the phase shift induced by the ionosphere over the $\Delta f = 1$ MHz bandwidth of the radar chirp signal is substantial, approximately 200 rad for a centre frequency at $f = 2f_p$(max), and 5 rad at

$f = 10\,f_p(\max)$. Since the sounder must almost certainly operate at frequencies below $10\,f_p(\max)$, it follows that we must be prepared to remove the dispersive effects of the ionosphere, otherwise the signal-to-noise ratio and range resolution of the radar signal would be severely degraded in the chirp compression process.

5. MARSIS Orbital Requirements

The baseline orbit for Mars Express has a periapsis distance of 250 km, apoapsis distance of 10 142 km, inclination 86.35° and period of 6.75 h. Figure 3 shows the tangential and radial components of the satellite's orbital velocity as a function of altitude above the equatorial radius. MARSIS is designed to perform subsurface sounding during each orbit when the altitude is lower than about 800 km; for the baseline orbit that means a period of about 26 min. This allows mapping of about 100° on the surface on each orbit, allowing extensive coverage at all latitudes within the nominal mission duration. To achieve this global coverage, MARSIS is designed to support both dayside and nightside operations, although performances are maximised during the night (solar zenith angle > 80°), when the ionosphere plasma frequency drops off significantly and the lower frequency bands, which have greater penetration capability, can be used. Ionospheric soundings will be also carried out by MARSIS on certain passes when the orbiter is at an altitude up to 1200 km, both during day and night time.

6. Measurement Concept and Experiment Description

6.1 Subsurface and surface sounding

The sounder's principle of operation is explained in Fig. 4. The electromagnetic wave transmitted by the antenna impinges on the surface, producing a first reflection that propagates back to the radar, generating a strong return signal received at time $t_0 = 2H/c$, H being the spacecraft height and c the speed of light in vacuum. However, thanks to the long wavelengths employed, a significant fraction of the energy impinging on the surface is transmitted into the crust and propagates down with a decreased velocity $v = c/n$ (n is the refractive index of ice related to the real dielectric constant ε_r by $n = \sqrt{\varepsilon_r}$) and an attenuation proportional to the penetration depth (z), to the wavelength (λ) and to the material loss tangent ($\tan\delta$, defined as the ratio of the imaginary part to the real part of the complex dielectric constant, $\tan\delta = \varepsilon_i/\varepsilon_r$). Should subsurface dielectric discontinuities be present at depth z_0 below the surface, additional reflections would occur and the echoes would propagate back through the first layer medium and then to the radar, generating further echo signals, much weaker than the front surface signal, with time delay $t_0 + 2z_0/v$. As a consequence, time-domain analysis of the strong surface return, eventually after multi-look non-coherent integration, allows estimation of surface roughness, reflectivity and mean distance, just as in classical pulse-limited surface radar altimeters. Moreover, the weaker signals after the first strong surface return will enable the detection of subsurface interfaces, while their time delays will allow measurement of the depths of those interfaces.

Detection performance will be limited by two main factors: the strength of the surface clutter echoes and the noise floor entering the receiver. The surface clutter echoes originate by reflections from those surface areas (marked C in Fig. 4) that have 2-way propagation path delays identical to that of the useful subsurface signal (point B in Fig. 4). While this is not a problem for perfectly flat surfaces (the angular backscattering law imposes a very high attenuation on such lateral reflections), most natural surfaces are not at all flat and surface clutter echoes can be very strong in practical situations. As a direct consequence, when the competing subsurface echoes are highly attenuated by the propagation into the crust, the surface clutter echoes may mask the useful signal and limit the detection. Furthermore, even when the surface clutter power is lower than the competing subsurface echo, the detection performance can be limited by the noise floor of the receiver. Such noise can be very high at the low frequencies commonly used for radar sounding owing to the contribution of the cosmic noise temperature entering the receiver, which is many order of magnitudes

Fig. 3. Radial and tangential spacecraft velocity.

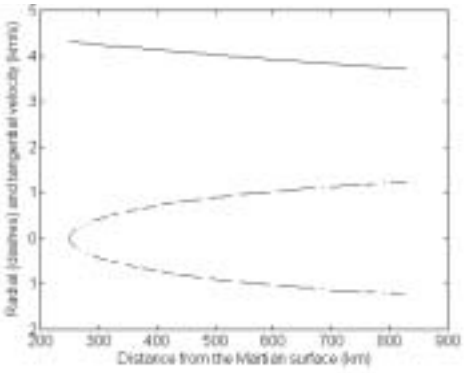

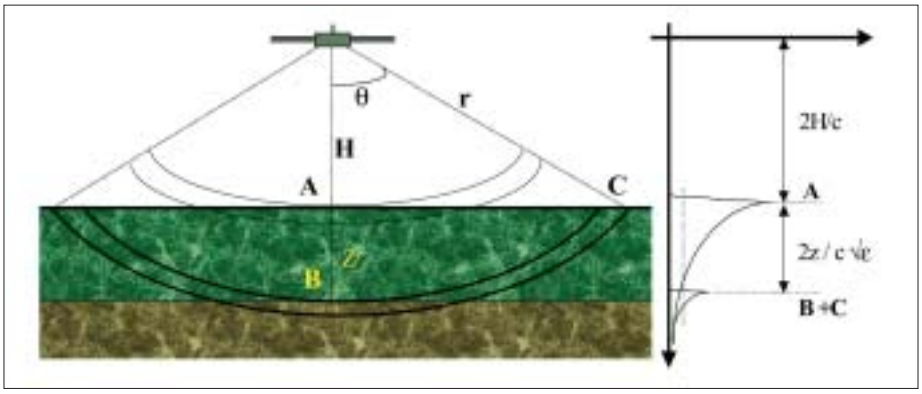

Fig. 4. MARSIS observation geometry and principle of operation.

higher than receiver internal noise for typical noise figures of 3-4 dB and frequencies of 1-10 MHz (Picardi et al., 1998a; 1999a).

In the standard subsurface sounding mode, MARSIS can transmit and receive any of the following bands: 1.3-2.3 MHz (centred at 1.8 MHz), 2.5-3.5 MHz (centred at 3 MHz), 3.5-4.5 MHz (centred at 4 MHz) and 4.5-5.5 MHz (centred at 5 MHz). The instantaneous bandwidth is 1 MHz for all the bands, and the transmitted waveform is a pseudo-linear frequency modulated pulse (chirp). Since, on the dayside of Mars, the ionosphere will not allow the use of frequencies below ~3 MHz, only the two higher bands (4 MHz and 5 MHz) can be used for surface/subsurface sounding during the day. However, the best penetration is during nightside observations, when the longest wavelengths can also be used.

Transmitted pulses are radiated through a 40 m tip-to-tip dipole mounted normally to the orbiter's direction of motion, fed by a matching network that flattens the antenna frequency response over the full 1.3-5.5 MHz range. The reflected echoes are received both from the primary dipole antenna and from a secondary receiving antenna. This short monopole is mounted vertically, aligned with the nadir axis, and features a null in the nadir direction and thus records off-nadir surface echoes alone (Picardi et al., 1999b). Received echoes on both channels are converted to a small offset frequency and digitised for onboard processing and later downlink. The receiving window accommodates echoes from a maximum depth of 5-8 km, depending on the crust dielectric constant. Since the data rate of the digitised samples is on the order of a few Mbit/s, substantial data reduction is performed onboard to comply with the orbiter's data rate and volume constraints. Data reduction is performed by the onboard processor, which features adaptive range compression, azimuth compression and multi-look non-coherent integration, depending on the operating modes. The range compression allows a range resolution equivalent to 150 m in vacuum and waveform sidelobes controlled to provide a system dynamic range in excess of 50 dB. Azimuth compression is performed by coherent unfocused Doppler processing, to reduce along-track surface clutter and noise power; the along-track resolution after azimuth compression is sharpened to 5-9 km, depending on the altitude. Cross-track surface clutter reduction by dipole/monopole signal combination is performed during ground processing. Non-coherent averaging with multiple Doppler filters (looks) can also be performed before downlink to reduce statistical fluctuations of the final profiles. Finally, echo profiles collected at different frequencies can be processed to enhance the discrimination of subsurface reflections, which are strongly dependent on the frequency, from the surface reflections, which are mostly frequency-independent.

During ground processing, downlinked data will be analysed for time delay to subsurface reflector(s), intensity of subsurface reflection(s), and a measure of 'confidence' that a subsurface interface was detected. These parameters will be incorporated into a global map database, to allow interpretation of local and regional behaviour. Detailed analysis will be conducted for regions of interest. This will include modelling of the electrical properties of the layers and interfaces. The modelling will

result in estimates of thickness of layers, depth to interfaces, dielectric properties of the materials, and an interpretation of the properties of the materials, including composition. It is expected that the abrupt dielectric contrasts that should exist at a martian water table would allow an unambiguous identification of liquid water. If small (tens of km in lateral extent) aquifers are present, the resolution and processing scheme of MARSIS should allow their detection, unlike other systems that may require extensive, uniform layer and interface conditions. Boundaries involving the presence and absence of ground-ice will be more difficult to distinguish, but regional trends (with latitude and elevation) should allow discrimination of ground-ice boundaries.

The first surface reflection echoes of MARSIS operating as a sounder will be processed to give estimates of the average height, roughness and reflection coefficient of the surface layer, according to the classical altimetric approach. By measuring the time delay of the echo, it will be possible to estimate the average distance of the radar from a reference flat surface level, while the duration of the waveform leading edge will be proportional to the large-scale surface roughness averaged over the pulse-limited spatial resolution cell. Finally, the peak value of the average echo waveform will be used to estimate the backscattering coefficient and, in conjunction with the roughness value, to estimate the Fresnel reflection coefficient of the surface. A further improvement of the altimeter mode performance, in terms of resolution and accuracy, can be achieved by processing the return echoes collected over the same region during different orbits. During ground processing, surface reflection profiles will be analysed for surface reflectivity at each frequency, echo dispersion at the surface (an indication of surface roughness) and surface elevation. These parameters will be further incorporated into the global map database, to allow interpretation of local and regional behaviour, and for comparisons with other data sets.

6.2 Ionospheric sounding

MARSIS ionospheric measurements employ both passive and active techniques. The passive technique uses the thermal emission line at the local electron plasma frequency to make highly accurate measurements of the local electron density. The active technique uses radar signals (soundings) to measure the vertical range to the ionospheric reflection point as a function of frequency. For active soundings, a simple ionospheric mode of operation is used in which sinusoidal pulses with a nominal duration of 91.4 ms are transmitted in 160 frequency steps from 0.1 MHz to 5.4 MHz. The time required to step through a complete frequency sweep is 1.23 s. Using these measurements, the vertical profile of the plasma electron frequency (hence, electron density) can be determined, as in Fig. 2a. There are two modes of operation: continuous and interleaved. The continuous mode of operation provides a contiguous series of ionospheric sounding sweeps, thereby providing the highest possible horizontal resolution. Since such a contiguous series of sweeps leaves no time for subsurface soundings, this mode is used relatively infrequently. The more common mode interleaves the subsurface soundings with the ionospheric soundings in a regular pattern. These will be particularly useful if ionospheric electron density information is needed to interpret or optimise the subsurface soundings.

7. Instrument Description

A functional block diagram of MARSIS is shown in Fig. 5; the principal characteristics are given in Table 3. There are three main subsystems:

— the Antenna Subsystem (AS), including the primary dipole antenna for transmission and reception of the sounder pulses, and the secondary monopole antenna for surface-clutter echo reception only;
— the Radio Frequency Subsystem (RFS), including both the transmit channel and the two receive channels for the dipole and monopole antennas, respectively;
— the Digital Electronics Subsystem (DES), including the signal generator, timing and control unit and the processing unit.

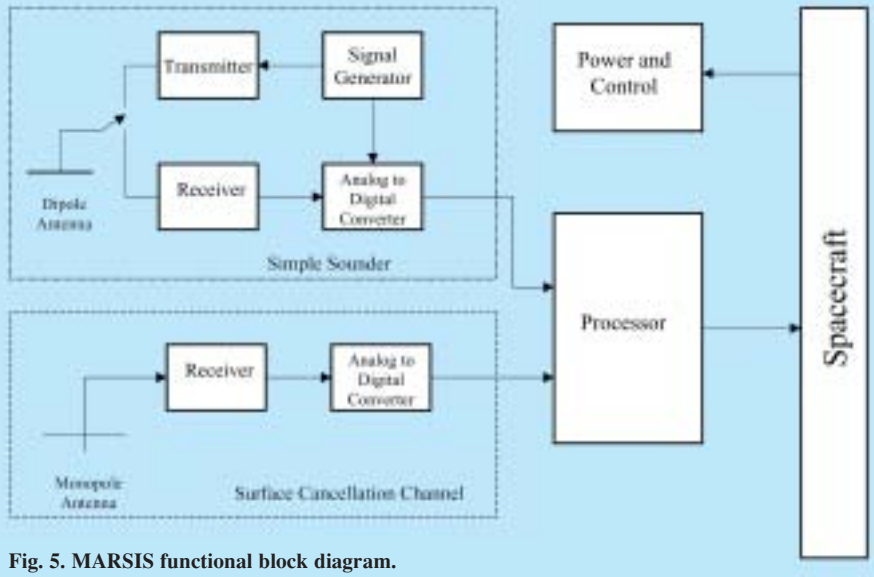

Fig. 5. MARSIS functional block diagram.

Table 3. Principal parameters for the MARSIS subsurface sounding mode.

Centre frequencies	
Band 1	1.8 MHz
Band 2	3.0 MHz
Band 3	4.0 MHz
Band 4	5.0 MHz
Bandwidth	1.0 MHz
Irradiated power	
Band 1	1.5 W
Band 2	5.0 W
Band 3	5.0 W
Band 4	5.0 W
Transmit pulse width	250 µs (30 µs in mode SS5)
PRF	130/s
Minimum altitude	250 km
Max. altitude subsurface sounding	800 km
Max. altitude ionosphere sounding	1200 km
Receive window size per channel (baseline)	350 µs
Analog to digital conversion rate	2.8 MHz
Analog to digital conversion	8 Bit
No. processed channels	4 (max)
Max. no. simultaneous frequencies	2
Radiation gain	2.1 dB
Dipole antenna element length	20 m
Monopole antenna length	7 m
Data rate output (min/max)	18/75 kbit/s
Data volume daily (max)	285 Mbit
Mass	17 kg
Power (max. incl. margins)	64.5 W

In nominal surface/subsurface sounding operations, MARSIS transmits in rapid sequence up to four quasi-simultaneous pulses at one or two different frequencies, selected from the four available bands, and receives the corresponding echoes on both the dipole and monopole antennas. The whole transmit/receive cycle is repeated at a rate fixed by the system Pulse Repetition Frequency (PRF). The selection of the PRF is an important issue in the definition of the MARSIS timing scheme, since the antenna pattern is practically isotropic in the along-track direction. With this system, spectral aliasing of surface clutter echoes could occur if the Doppler bandwidth is under-sampled. Considering that a folding localised into far-range cells can be accepted at the highest frequency bands (because penetration to the corresponding depths is unlikely) a fixed PRF of 130 Hz was selected as the baseline for surface/subsurface sounding. In fact, the risk of folding in useful range cells seems to be very small, while the implementation burden is significantly reduced. With such a PRF, the basic transmit/receive repetition interval is 7.69 ms. Within this time frame, the MARSIS transmitter radiates through the main dipole antenna up to four chirps of nominal duration 250 µs, waiting for about 100 µs between any two consecutive chirps. Two different frequency bands can be assigned to the four pulses, selectable from the four operating bands. After transmission is completed, MARSIS turns to the receive mode and records the signals received from both dipole and monopole channels for each transmitted pulse. The duration of the receiving window 350 µs, accommodating an echo dispersion of about 100 µs, which corresponds to about 5-8 km of penetration, depending on the propagation velocity in the crust. Upon reception, echoes are down-converted and digitised to a format suitable for the onboard processor. Four processing channels allow the processing of two frequency bands received from the dipole and monopole at each PRF. The digitised echo stream is processed by the digital electronics subsystem in order to reduce the data rate and data volume, and allow global mapping of the observed scene within the allocated amount of orbiter mass memory.

Starting from the desired along-track sampling rate of the surface, the basic azimuth repetition interval is identified and all the pulses received within such an interval (frame) are processed to yield a single echo profile referring to one azimuth location. Range compression is performed on each pulse by classical matched filtering, although adaptive techniques are used to update the matched filter reference

function at each frame in order to correct for the time-variant phase distortions introduced by the ionosphere propagation (Picardi et al., 1998a; 1999a; Picardi & Sorge, 1999). The information needed for this adaptive filtering is estimated by a dedicated processing of the initial pulses of each frame, and is then used for all the remaining pulses of the same frame, thus assuming the fluctuation rate of the distortion is slower than the frame duration. Alternative techniques for such adaptive filtering are based either on using the front surface reflection for direct extraction of the propagation medium's impulse response (Safaeinili & Jordan, 2000), on the estimation of some parametric model of the propagation medium using a contrast maximisation technique (Picardi & Sorge, 1999; Biccari et al., 2001c).

By correctly sampling the surface and subsurface Doppler spectra, coherent integration of the range-compressed echoes within each frame is possible, enhancing the spatial resolution in the along-track direction and linearly reducing the cosmic noise level (Picardi et al., 1998a: 1999a). For simplicity, unfocused Doppler processing has been implemented, entailing an azimuth resolution of 5000 m at altitudes below 300 km, increasing to 9000 m at higher altitudes. Coherent integration is performed using a fixed number of phase-correction functions, thus synthesising a bank of parallel Doppler filters around the zero Doppler point (or the Doppler centroid). However, since the small amount of computational and memory resources available in the processor limits the number of Doppler filters that can be synthesised to about five, the position and usage of these filters are optimised taking into account the behaviour of the observed surface. Specifically, if specular scattering from a flat surface is dominant, the greatest portion of the echo power falls into the single Doppler filter that contains the point of specular reflection (the central Doppler filter for a non-tilted surface), leaving mostly noise to the lateral Doppler filters. Under such conditions, it is clear that the best choice is to use that single Doppler filter, eventually located by a Doppler-tracking algorithm, and discard the others. For the contrary case of a rough layer, non-coherent scattering is dominant and the signal power is distributed over several Doppler filters, so it is worth averaging echoes from the same zone processed by different Doppler filters to improve the signal-to-noise (S/N) ratio and reduce statistical fluctuations (speckle).

A primary indication of MARSIS' capability for subsurface sounding is given by the S/N at the processor's output (Picardi et al., 1999a). Under normal MARSIS operating conditions, the contribution of the receiver internal noise to the system noise temperature can be neglected, compared to the contribution of the external cosmic noise. This assumption is easily verified at low frequencies, where the cosmic noise temperature is millions of K, which corresponds to receiver noise figures higher than 40 dB.

The maximum dynamic range of the sounder can be computed by evaluating the S/N in the case of a rough surface, where the surface echo can be evaluated according to the geometric optics approximation, and in the case of a perfectly specular surface return, where the geometric optics approximation cannot be applied and we get a higher echo from the surface.

Evaluating the radar equation in the two cases shows that, during nominal sounding operations, an S/N always better than 14 dB is available on the front surface echo. This allows precise positioning of the receiving window using a tracking algorithm, and allows precise estimation of surface parameters with the surface altimetry mode, provided that sufficient averaging is performed to reduce statistical fluctuations of the signal (speckle noise).

8. Model Performance

To assess the interface-detection performance of the radar sounder, the backscattering cross-sections of concurrent echoes from the surface and subsurface layers (Fig. 4) as operating conditions change need to be evaluated. These can be expressed as $\sigma_s = \Gamma_s f_s(\sigma_{h,s}, L_s, \lambda)$ and $\sigma_{ss} = \Gamma_{ss} f_{ss}(\sigma_{h,ss}, L_{ss}, \lambda)$, with Γ_s and Γ_{ss} being the Fresnel reflectivity terms, which deal with the surface and subsurface dielectric properties, and f_s and f_{ss} the geometric scattering terms, which deal with the geometric structure

of the surface and subsurface; L_s and L_{ss} are the correlation lengths; λ is the wavelength. In the following sections, the Fresnel terms and the geometric scattering terms are evaluated using the simplified reference crust models introduced in Sections 2 and 3.

8.1 Modelling of Fresnel reflectivity terms

According to electromagnetic theory, the Fresnel reflectivity for nadir incidence on a surface can be expressed as:

$$\Gamma_s = \left| \frac{1 - \sqrt{\varepsilon_{r1}(0)}}{1 + \sqrt{\varepsilon_{r1}(0)}} \right|^2 = R_{01}^2 \tag{2}$$

with $\varepsilon_{r1}(0)$ the real dielectric constant of the crust evaluated at the surface ($z = 0$). The Fresnel reflectivity for the subsurface layer at depth z can be expressed as:

$$\Gamma_{ss,z} = R_{12,z}^2 (1 - R_{01}^2)^2 \, 10^{-0.1 \int_0^z \alpha(\zeta)\, d\zeta} \tag{3}$$

with $R_{12,z}^2$ the reflection coefficient of an interface located at depth z:

$$R_{12,z}^2 = \left| \frac{\sqrt{\varepsilon_{r1}(z)} - \sqrt{\varepsilon_{r2}(z)}}{\sqrt{\varepsilon_{r1}(z)} + \sqrt{\varepsilon_{r2}(z)}} \right|^2 \tag{4}$$

and $\alpha(\zeta)$ the 2-way unit depth attenuation due to dielectric dissipation in the crust, expressed in dB/m:

$$\alpha(\zeta) = 1.8 \times 10^{-7} f_0 \sqrt{\varepsilon} \tan \delta \tag{5}$$

The evaluation of the Fresnel reflectivity terms requires knowledge of the complex dielectric constants of the crust as a function of depth. This can be modelled starting from the dielectric constants of the basic elements contained in the martian crust (Table 1) and using the exponential law (Eq. 1) for the porosity decay against the depth into well-known Host-Inclusion mixing formulae (Picardi et al., 1999a). Since porosity depends on depth, then so do the effective dielectric constants of the mixtures. The Maxwell-Garnett model for spherical inclusions was adopted for this analysis. As a result, the real dielectric constant at the surface (a water-filled regolith is not considered to be possible at the surface) ranges between 4 and 6 for a basalt-like regolith, and between 2 and 4 for andesite-like regolith; the lower values correspond to higher surface porosity and dry regolith. As the depth increases, the first layer's dielectric constant increases because of the lower porosity and approaches the dielectric constant of the pure host material (basalt or andesite in our models). If an interface among ice-filled and water-filled regolith or dry-regolith and ice-filled regolith occurs at a certain depth, there will be an abrupt change in the real part of the dielectric constant. The dielectric contrast will be higher for ice/water interfaces, for higher surface porosity and, of course, for greater depths. This dielectric contrast is the origin for the subsurface reflection process, and the subsurface reflection coefficient will be proportional to its intensity through Eq. 4. Moreover, the absorption in the crust can be modelled using Eq. 5 and the obtained loss tangent profiles and the total subsurface reflectivity can be computed by performing integration over the depth according to Eq. 3. Figure 6 shows the resulting reflectivity of the surface and subsurface echoes for both ice/water and dry/ice interface scenarios, assuming the different materials and surface porosity values listed in Table 1. It is clear from the figures that the surface reflectivity ranges between –7 dB

and –15 dB, depending on the surface composition and porosity, and has a typical value of –10 dB for most scenarios.

8.2 Backscattering model

As mentioned in Section 3, backscattering from the martian surface can be modelled by considering two main terms: the large-scale scattering contribution results from gentle geometrical undulations of the surface on a scale of many hundreds to thousands of metres, whereas the small-scale scattering contribution arises from the rapid, slight variations of surface height over a horizontal scale of some tenths of metres. Both surface scales are modelled as Gaussian random processes with a circular symmetric correlation function, and are described by the rms height σ_h and correlation length L. A third non-independent parameter is introduced, called rms slope, which for a Gaussian correlation function is given by $m_s = \sqrt{2}\sigma_h/L$ and represents the average geometric slope of the surface.

Simple approximate methods can be applied for surfaces that present a unique roughness scale, with either a large correlation length (gently undulating surface) or a very small rms height (slightly rough surface) compared to the incident wavelength. Specifically, the Kirchhoff method can be applied for gently undulating surfaces, which respect the tangent plane conditions, and the Small Perturbation Method can be applied to slightly rough surfaces. The classical studies on the validity conditions of these two models have recently been updated, and regions of validity currently defined show that the Kirchhoff approximation can be used to evaluate the large-scale backscattering contribution, whereas the Small Perturbation Method can be used for the small-scale contribution. The approach here for modelling the total surface backscattering is to consider the two roughness scales independently and to sum the respective backscattering cross-sections obtained with the Kirchhoff and Small Perturbation Method approximations.

For the Kirchhoff term, an analytic model of the backscattering cross-section was obtained by extending the electric field method followed by Fung & Eom (1983) to the case of a generic Kirchhoff surface and pulsed radar. The expression found allows prediction of the backscattering cross-section without restriction to the geometrical optics approximation (pure diffuse scattering), but properly taking into account both the coherent (specular) and non-coherent (diffuse) component of the scattering process. Under the simplifying assumptions of a Gaussian surface correlation function and Gaussian (compressed) pulse shape, the expression of the Kirchhoff backscattering cross-section is:

$$P_K(\tau) = \Gamma \pi H^2 (P_c + P_{nc1} - P_{nc2}) \quad (6)$$

where H is the altitude, $P_c(\tau)$ is the coherent (specular) scattering component, while $P_{nc}(\tau) = P_{nc1}(\tau) - P_{nc2}(\tau)$ is the non-coherent (diffuse) scattering component.

The maximum power is received when full coherent reflection occurs, i.e. when the surface is perfectly flat. In such a condition, it is easy to verify that $P_{nc1} = P_{nc2}$ and the non-coherent term P_{nc} reduces to zero, while the coherent term P_c approaches the shape of the transmitted pulse, which is maximum in the origin; the maximum cross-section of the large-scale contribution of the surface is then $\sigma_{K,max} = \Gamma \pi H^2$, which is a value consistent with that predicted by the image theorem for the reflection coefficient of perfectly flat surfaces. As the surface becomes rougher, the coherent component goes towards zero and non-coherent scattering becomes dominant (geometrical optics model). By considering the fractal surface model (Section 3), the geometric optics model ($H = 1$ in the fractal model) can be considered as the end model. Moreover, the Hagfors model ($H = 1/2$ in the fractal model) will be the other end-model: the geometric optics model is considered as the worst case (Biccari et al., 2001a).

Turning to the small-scale contribution, the Small Perturbation Method approximation allows the backscattering coefficient to be expressed as:

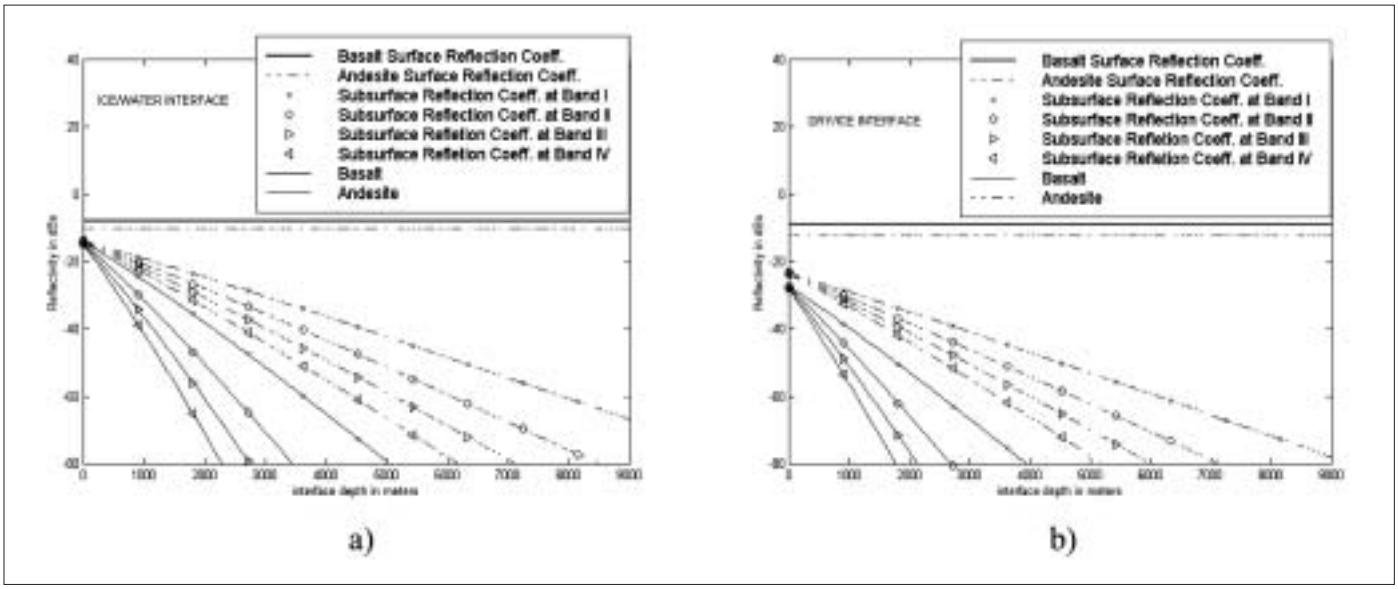

Fig. 6. Surface and subsurface Fresnel reflectivity with medium surface porosity (35%) and (a) ice/water interface, (b) dry/ice interface.

$$\sigma^0_{pp}(\theta) = 8k^4\,\sigma^2_{h2}\,|\alpha_{pp}(\theta)|^2\cos^4 q\;W(K_B) \tag{7}$$

where $k = 2\pi/\lambda$ is the wave number, θ is the incidence angle, $a_{pp}(\theta)$ is the Fresnel Reflection Coefficient for the pp polarisation, $W(K)$ is the surface roughness small-scale spectrum and K_B is the Bragg Frequency, given by $K_B = 2k\sin\theta$.

Summarising, the surface backscattered power, $\sigma_T(\tau)$, can be obtained by summing the large-scale and small-scale contributions:

$$\sigma_T(\tau) = \sigma_K(\tau) + \sigma_{SP}(\tau) \tag{8}$$

where $\sigma_{SP}(\tau)$ is the Small Perturbation term. Figure 7 shows the surface cross-section given by Eq. 8, assuming the worst-case small-scale contribution and a large-scale correlation length of about 2000 m, as a function of the depth of the competing subsurface return (assuming a reference average $\varepsilon_r = 4$). The plots are normalised so that the 0 dB axis indicates the maximum possible cross-section, which is given again by $\sigma_{K,max} = \Gamma\pi H^2$. As seen in the figure, the scattering cross-section is maximum at nadir and rapidly falls as the 'equivalent depth' increases, up to a level at which it becomes practically a constant. This behaviour can be easily understood by considering the superposition of the two scale contributions. In fact, according to classical random scattering theory, the large-scale Kirchhoff component dominates the backscattering around the nadir and determines the cross-section fall-off rate (owing to the small value of m_s), while the small-perturbation component dominates at high off-nadir locations and is responsible for the flat behaviour of the cross-section when the Kirchhoff contribution has vanished.

8.3 Surface clutter reduction techniques

As apparent from Fig. 7, when sounding over rough areas of the martian crust (rms slope > 2-3°) the detection depth will be severely limited by the surface clutter, rather than by the cosmic noise. In order to improve the sounding performance in these regions, different methods of reducing the surface clutter contributions were included in MARSIS: Doppler filtering of surface clutter; dual-antenna clutter cancellation; and dual-frequency clutter cancellation. Detailed descriptions and performance assessment of the three methods can be found in Picardi et al. (1999a). Below is a short review of the techniques and their cancellation performances.

Doppler filtering of the surface clutter is a direct consequence of the azimuthal synthetic aperture processing performed by the MARSIS onboard processor to

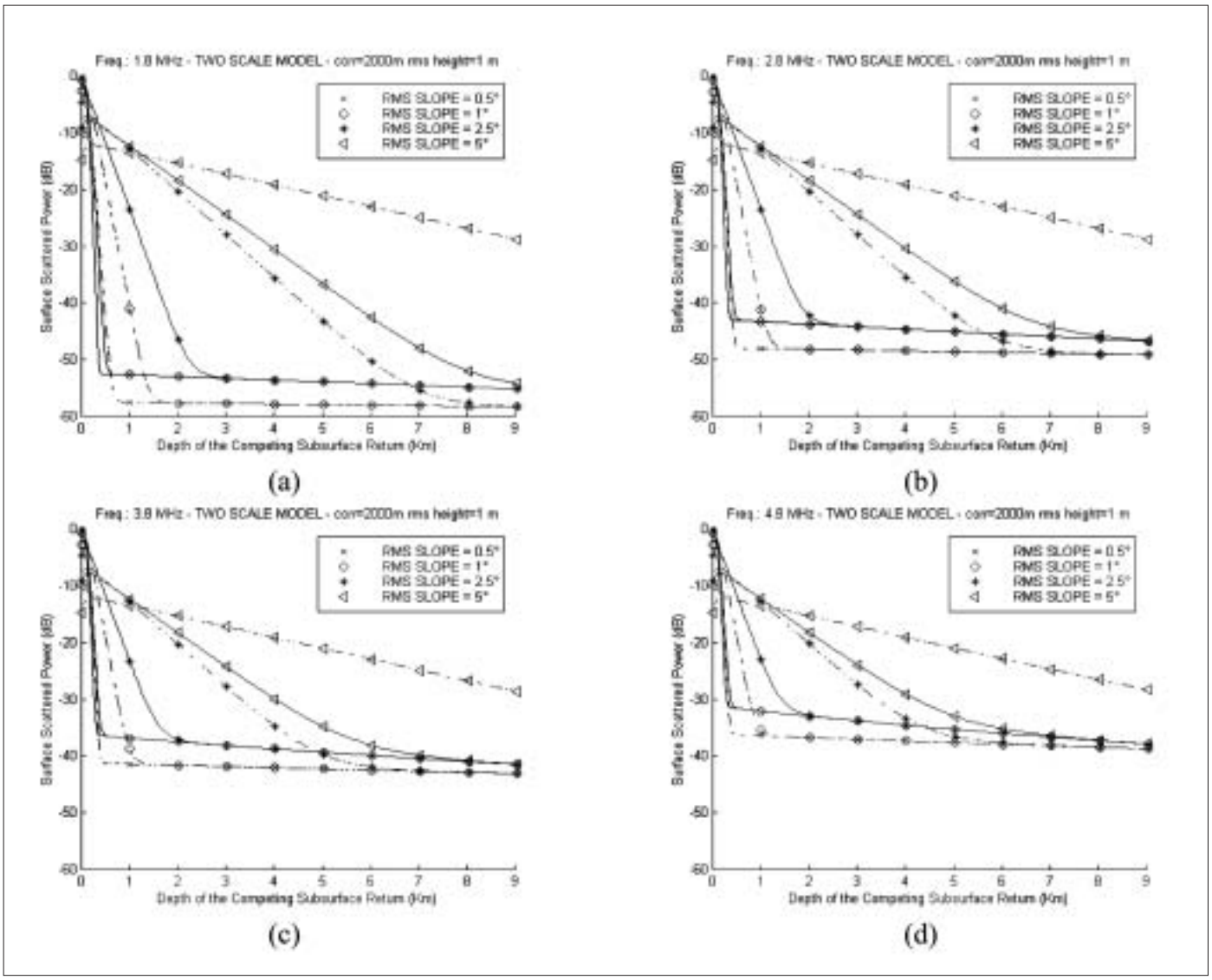

Fig. 7. Surface scattered power according to the two-scale model. A Gaussian spectrum at large-scale and a 1.5-power law spectrum at small-scale are assumed. Large-scale correlation length is 2000 m, small-scale rms height is 1 m. *H* = 250 m (-) and 800 km (-.-.). a: 1.8 MHz; b: 2.8 MHz; c: 3.8 MHz; d: 4.8 MHz.

sharpen the along-track resolution and enhance noise suppression. In fact, if the Doppler spectrum at each specific range location is sampled using a proper PRF, the surface clutter contribution from along-track off-nadir angles is mapped to the high end of the Doppler spectrum, while subsurface echoes from nadir are mapped to the lowest portion of the Doppler spectrum.

The amount of clutter reduction from this technique can be evaluated by simple geometric considerations, taking into account the reduction of the scattering areas for the nadir subsurface return and the off-nadir surface return, after Doppler filtering. An improvement factor (IF) can be defined as the ratio of signal-to-clutter ratios before and after the cancellation technique. The Doppler filtering IF can be expressed approximately by:

$$\mathrm{IF} = \sqrt{\frac{z}{\Delta}}\left(1 - \sqrt{1 - \frac{\Delta}{z}}\right) \tag{9}$$

where z is the depth of the subsurface return and Δ is the radar range resolution, and the condition $z > \Delta$ is assumed to be verified. As clearly seen in Fig. 8a, an IF of about 12 dB can be obtained by this technique at large depths.

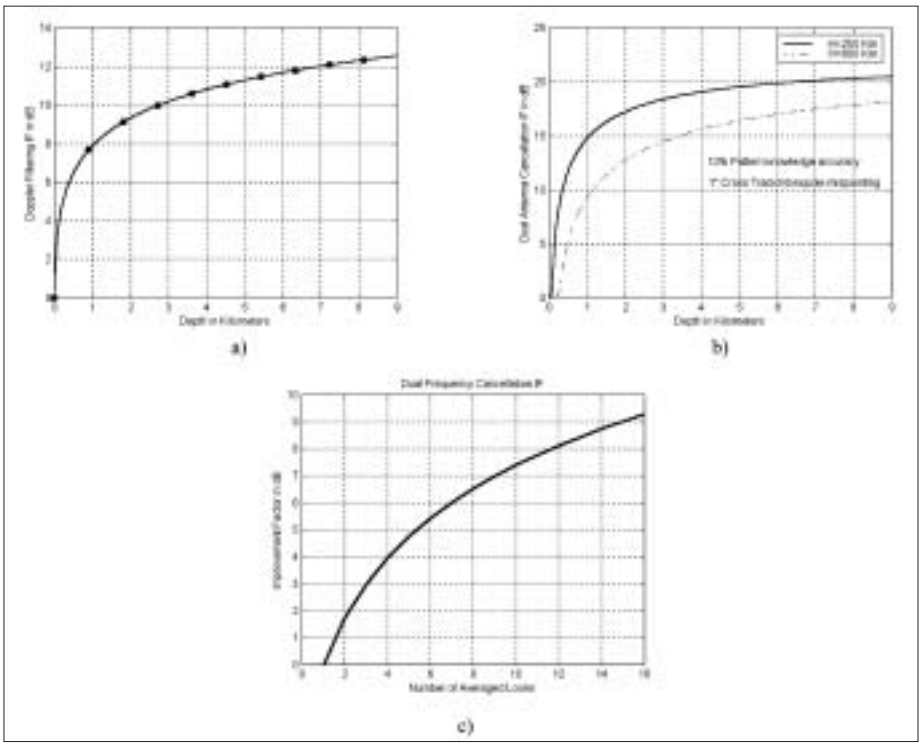

Fig. 8. Improvement Factor (IF) of the surface clutter cancellation techniques. a: Doppler filtering; b: dual-antenna cancellation (1° roll angle and 10% antenna pattern knowledge accuracy); c: dual-frequency cancellation as a function of number of averaged looks.

Since surface clutter echoes from off-nadir in the cross-track direction are not affected by any Doppler modulation and cannot be eliminated by the previous technique, additional clutter suppression techniques were studied for MARSIS, based on a dual-antenna or dual-frequency processing concept.

The dual-antenna cancellation technique (Picardi et al., 1998a; 1999a) uses a primary antenna to transmit and receive the composite subsurface/surface signal, with a pattern maximum in the nadir direction (for MARSIS, a dipole mounted parallel to the surface and normal to the motion direction) and a secondary antenna to receive surface clutter only, with a pattern null in the nadir direction (for MARSIS, a short monopole oriented vertically under the spacecraft). The cancellation scheme is a coherent subtraction after correction for the antenna gain imbalance between the two channels:

$$V_{\text{tot}} = V_1 - V_2 \sqrt{\frac{G_1(\theta)}{G_2(\theta)}} \tag{10}$$

with V_1 and V_2 the complex signals at the dipole and monopole channels, and $G_1(\theta)$ and $G_2(\theta)$ the antenna gain patterns for the dipole and monopole, respectively. It is simple to show (Picardi et al., 1999a) that the surface clutter echoes are completely removed by the subtraction, leading to infinite IF, if we assume that:

— returns from the two antennas are totally correlated;
— surface and subsurface return contributions to V_1 and V_2 are totally uncorrelated;
— the antenna patterns $G_1(\theta)$ and $G_2(\theta)$ are perfectly known;
— the monopole pattern null points exactly towards the nadir direction in both along-track and cross-track directions;
— the primary and secondary antenna channels have the same phase/amplitude transfer function (perfectly amplitude-balanced and phase-matched channels).

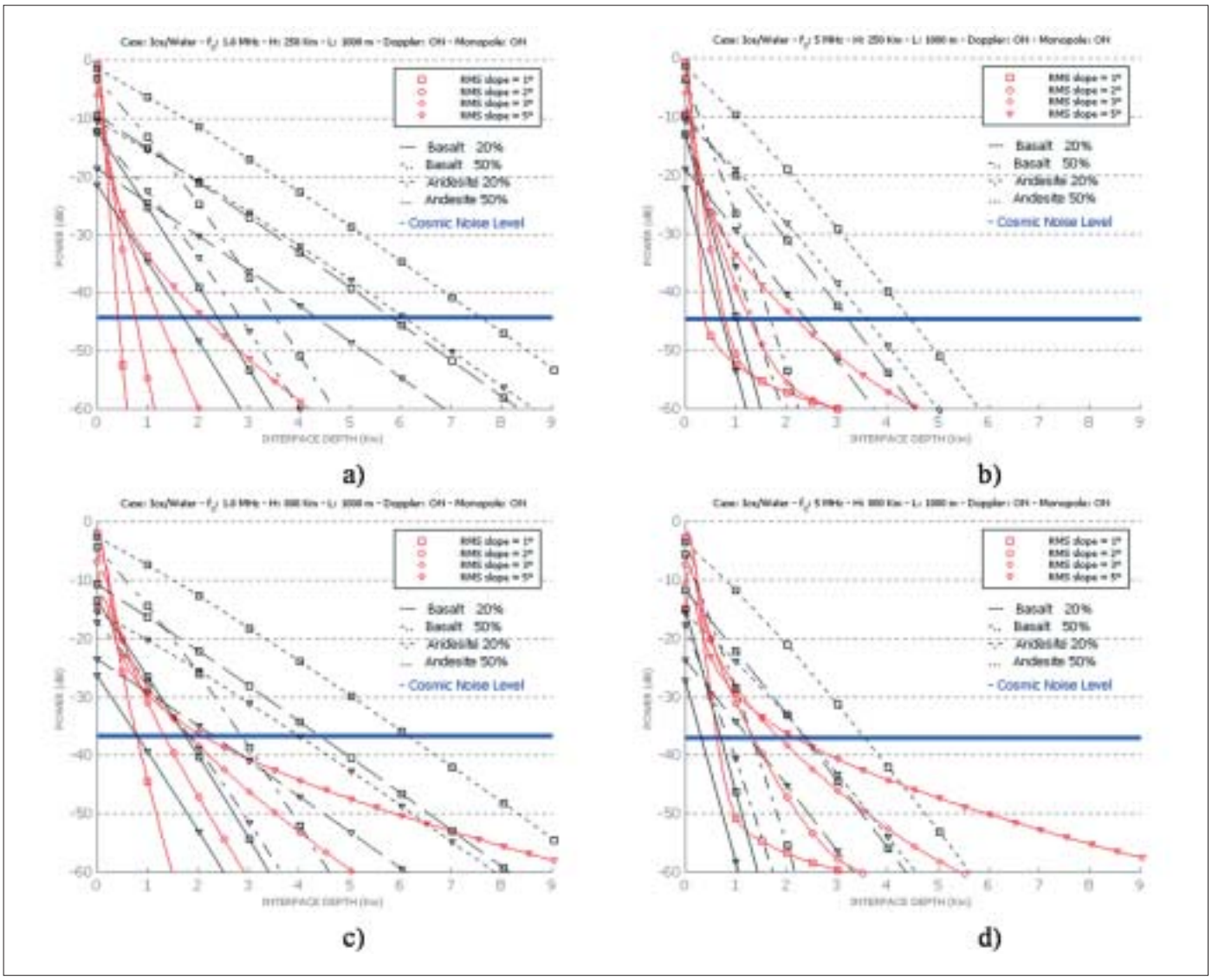

Fig. 9. Ice/Water interface detection charts. Subsurface attenuation (including absorption and scattering loss) appears in black; surface clutter after coherent cancellation in red; noise floor in blue. Altitudes are *H* = 250 km and 800 km; frequencies are 1.8 MHz and 5 MHz. Surface correlation length is 1000 m.

In practice, the dual-antenna cancellation IF is limited by imperfect knowledge of the antenna pattern, unknown antenna pointing errors (roll and pitch angles) and amplitude/phase mismatching between the two channels. In Picardi et al. (1999a), these effects were considered and it was concluded that the main limitation to the IF comes from the antenna pattern knowledge and the cross-track pointing error of the monopole (roll angle).

Typical IF behaviour as a function of the antenna gain variance σ_g^2 and the spacecraft roll angle α is shown in Fig. 8b. Values of 10% accuracy in the knowledge of the antenna patterns and ±1° roll angle result in a maximum IF of about 20 dB. Note that this clutter cancellation technique could also be performed on the square-law detected signals on the two dipole and monopole channels, but with reduced performance.

Another technique for clutter suppression, based on non-coherent processing of echoes acquired simultaneously at different frequencies, has been proposed (Picardi et al., 1999a), in order to provide surface clutter cancellation if the dual-antenna technique proves insufficient (for example, owing to problems in positioning the monopole null) or cannot be applied because monopole channel data are not available on the ground. The dual-frequency technique uses the fact that the surface clutter

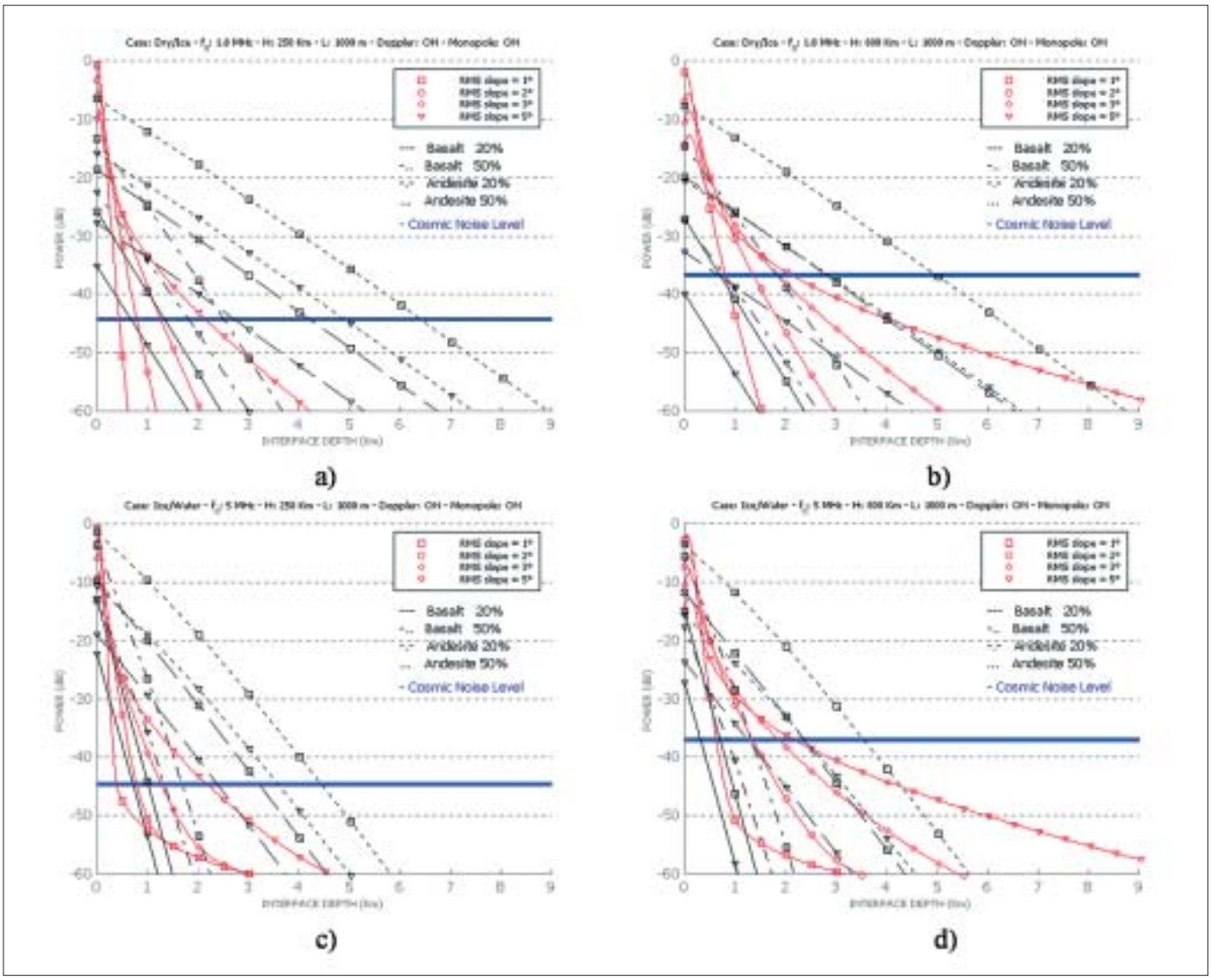

power at two frequencies remains almost constant (or the changes can be easily predicted by modelling), while the subsurface power is a strong function of frequency. As consequence, if the detected signals at both frequencies are subtracted, the surface contribution is significantly reduced while the subsurface contribution remains unchanged. The main limitation of this technique arises from the speckle which decorrelates at the two frequencies, and represents a clutter residual after cancellation. If the mean powers of surface clutter at the two frequencies are assumed to be equal, IF can be shown to be linearly related to the number of averaged looks before subtraction of the signal (Picardi et al., 1999a). As clearly seen in Fig. 8c, an IF of about 5 dB can be obtained using five averaged looks.

Fig. 10. Dry/Ice interface detection charts. Subsurface attenuation (including absorption and scattering loss) appears in black; surface clutter after coherent cancellation in red; noise floor in blue. Altitudes are H = 250 km and 800 km; frequencies are 1.8 MHz and 5 MHz. Surface correlation length is 1000 m.

8.4 Subsurface return signal-to-noise performance

Figures 9-10 summarise the predicted performance of the radar sounder in detecting the ice/water and dry/ice subsurface interfaces, according to the simple models described above and using the nominal MARSIS design parameters discussed in Section 6.1. Figure 9 refers to ice/water interface detection, and Fig. 10 to dry/ice. The four graphs in each figure present the detection at the two boundary frequency

bands (1.8 MHz and 5 MHz) from two altitudes (250 km and 800 km), which represent the minimum and maximum heights of Mars Express during the portion of the orbit when MARSIS is active. Each detection chart contains the following normalised power levels as a function of the interface depth:

— subsurface return power, including effects of absorption and scattering. Absorption is taken into account as in Section 8.1, assuming the two end-member host materials (basalt and andesite) and porosities (20-50%). The backscattering is computed assuming a subsurface correlation length equal to 2000 m and two extreme values of the subsurface layer rms slope (1° and 5°);
— surface clutter power after coherent clutter cancellation, including Doppler filtering and dual-antenna cancellation (dual-frequency cancellation is not considered because we want to evaluate single-look performance). Two values of rms slope are used, between 1° and 5°, while the surface correlation length is also assumed to be 2000 m;
— noise floor level, computed to match the S/N values reported in Section 8.2, plus a little increment from the receiver internal noise amplification after the dual-antenna cancellation.

Based on a 0 dB detection threshold criterion, it is easily seen from the figure that, thanks to the surface clutter cancellation techniques and to the strong noise suppression, penetration depths to several kilometres can be achieved under the most likely scenarios for the martian crust.

9. Ionospheric Sounding Performance

Since the ionosphere is a very good specular reflector, the S/N for active ionospheric sounding is expected to be good. The main difficulty is that, at frequencies below the half-wavelength resonance of the antenna (~3 MHz), the radiated power decreases rapidly with decreasing frequency (approximately as frequency to the fourth power). This is compensated for to some extent by the fact that the range to the ionospheric reflection point decreases with decreasing frequency (Fig. 2a), which tends to improve the S/N at low frequencies. Also, at frequencies below ~1 MHz, the cosmic noise background falls with decreasing frequency, which also improves the S/N at low frequencies. At a spacecraft altitude of 500 km, the resulting S/N for the daytime ionospheric model shown in Fig. 2a is expected to be 5.4 dB at 0.1 MHz, increasing to 8.6 dB at 0.3 MHz, 18.4 dB at 1.0 MHz and 21.3 dB at 3.0 MHz. These S/Ns are adequate to perform ionospheric sounding on the dayside of Mars under almost all conditions. On the night side, where the electron densities are expected to be much lower, the S/N is likely to become marginal, since the plasma frequencies are much lower, which increases the range to the reflection point for any given spacecraft altitude. It is also possible that the ionosphere may be more disturbed on the nightside of Mars, which could cause scattering from small-scale irregularities, thereby causing a further reduction in the S/N. Although the ionospheric sounding performance is somewhat marginal on the nightside, it is almost certain that useful information will be obtained, particularly at low altitudes where the range to the reflection point is very small. Also, a very strong return signal is expected when the sounding frequency passes through the local plasma frequency, which will give the local electron plasma density under almost all conditions.

References

Biccari, D., Picardi, G., Seu, R. & Melacci, P.T. (2001a). Mars Surface Models and Subsurface Detection Performance in MARSIS. In *Proc. IEEE International Symp. on Geoscience and Remote Sensing*, IGARSS 2001, Sydney, Australia, 9-13 July 2001.

Biccari, D., Ciabattoni, F., Picardi, G.,Seu, R., Johnson, W.K.T. Jordan, R., Plaut, J., Safaeinili, A., Gurnett, D.A., Orosei, R., Bombaci, O., Provvedi, F., Zampolini, E. & Zelli, C. (2001b). Mars Advanced Radar for Subsurface and Ionosphere Sounding (MARSIS). In *Proc. 2001 International Conference on Radar*, October 2001, Beijing, China.

Biccari, D., Cartacci, M., Lanza, P., Quattrociocchi, M., Picardi, G., Seu, R., Spanò, G. & Melacci, P.T. (2001c). *Ionosphere Phase Dispersion Compensation,* Infocom Technical Report N.002/005/01-23/12/2001.

Carr, M.H. (1996). *Water on Mars*, Oxford University Press, Oxford, UK.

Fung, A.K. & Eom, H.J. (1983). Coherent Scattering of a Spherical Wave from an Irregular Surface. *IEEE Trans. on Antennas and Propagation*, **AP-31**(1), 68-72.

Hanson, W.B., Sanatani, S. & Zuccaro, D.R. (1977). The Martian Ionosphere as Observed by the Viking Retarding Potential Analyzers. *J. Geophys. Res.* **82**, 4351-4363.

Picardi, G. & Sorge, S. (1999). *Adaptive Compensation of Mars Ionosphere Dispersion: A Low Computational Cost Solution for MARSIS*, Infocom Technical Report MRS-002/005/99, October 1999.

Picardi, G., Plaut, J., Johnson, W., Borgarelli, L., Jordan, R., Gurnett, D., Sorge, S., Seu, R. & Orosei, R. (1998a). *The Subsurface Sounding Radar Altimeter in the Mars Express Mission, Proposal to ESA,* Infocom document N188-23/2/1998, February 1998.

Picardi, G., Sorge, S., Seu, R., Fedele, G., Federico, C. & Orosei, R. (1999a). *Mars Advanced Radar for Subsurface and Ionosphere Sounding (MARSIS): Models and System Analysis*, Infocom Technical Rep. MRS-001/005/99, March 1999.

Picardi, G., Sorge, S., Seu, R., Fedele, G. & Jordan, R.L. (1999b). Coherent Cancellation of Surface Clutter Returns for Radar Sounding. In *Proc. IEEE International Symp. on Geoscience and Remote Sensing*, IGARSS'99, Hamburg, Germany, 28 June - 2 July 1999, pp2678-2681.

Safaeinili, A. & Jordan, R.L. (2000). Low Frequency Radar Sounding through Martian Ionosphere. In *Proc. IGARSS 2000*, 24-28 July 2000, Honolulu, Hawaii, IEEE, pp987-990.

Stix, T.H. (1964). *The Theory of Plasma Waves*, McGraw-Hill, New York.

Zhang, M.H.G., Luhmann, J.G., Kliore, A.J. & Kim, J. (1990a). A Post-Pioneer Venus Reassessment of the Martian Dayside Ionosphere as Observed by Radio Occultation Methods. *J. Geophys. Res.* **95**, 14,829-14,839.

Zhang, M.H.G., Luhmann, J.G., Kliore, A.J. & Kim, J. (1990b). An Observational Study of the Nightside Ionospheres of Mars and Venus with Radio Occultation Methods. *J. Geophys. Res.* **95**, 17,095-17,102.